ISSN 0021-8944, Journal of Applied Mechanics and Technical Physics, 2015, Vol. 56, No. 5, pp. 789–798. © Pleiades Publishing, Ltd., 2015.
Original Russian Text © K.N. Volkov, V.N. Emelyanov, M.S. Yakovchuk.

NUMERICAL SIMULATION OF THE INTERACTION OF A TRANSVERSE JET WITH A SUPERSONIC FLOW USING DIFFERENT TURBULENCE MODELS

K. N. Volkov, V. N. Emelyanov, and M. S. Yakovchuk

UDC 532.542.2

Abstract: This paper presents a numerical simulation of the flow resulting from transverse jet injection into a supersonic flow through a slot nozzle at different pressures in the injected jet and the crossflow. Calculations on grids with different resolutions use the Spalart–Allmaras turbulence model, the k–ε model, the k–ω model, and the SST model. Based on a comparison of the calculated and experimental data on the wall pressure distribution, the length of the recirculation area, and the depth of jet penetration into the supersonic flow, conclusions are made on the accuracy of the calculation results for the different turbulence models and the applicability of these models to similar problems.

Keywords: supersonic flow, jet, injection, turbulence, shock wave, numerical simulation.

DOI: 10.1134/S0021894415050053

INTRODUCTION

Transverse jet injection into a supersonic flow is of interest in the design of fuel and oxidizer mixing systems in supersonic combustion ramjet engines [1]. Jet injection into a supersonic flow is also employed in thrust vector control systems of solid-propellant rocket engines [2].

Mechanisms of interaction of jets of an incompressible liquid and a compressible gas with a crossflow are discussed in [3, 4]. The vortex flow pattern resulting from injection of subsonic jets is studied in [5–8]. A review of the issues and problems associated with the simulation of turbulence in high-velocity flows is given in [9].

Jet injection into a supersonic crossflow leads to the formation of the complex shock-wave vortex flow pattern shown in Fig. 1 [10]. The shock-wave flow structure includes a bow shock wave, which interacts with the boundary layer, two separation zones on the left and right of the injection slot, two barrel shock waves, a Mach disk, and a shock wave caused by repeated compression of the flow. In the recirculation zone upstream of the slot nozzle, vortices rotating in opposite directions are formed.

The region of jet penetration into the crossflow is limited by the barrel shock waves and the Mach disk. The angle of jet rotation depends on the crossflow velocity and the ratio of the pressure in the injected jet p_j and the crossflow p_∞ [11, 12]. A pair of vortices rotating in opposite directions is formed downstream of the bow shock wave [6]. The size of the vortex structures is determined by the type of the injected gas and the shape of the nozzle exit section [13]. The separation of the boundary layer and the formation of a recirculation zone upstream of the injection slot lead to the formation of a horseshoe vortex which envelopes the injected jet [12]. The size and number of the vortex structures formed in the flow separation region depend on the pressure gradient p_j/p_∞ [14]. For example, at large pressure gradients, four vortex structures are observed [15].

Ustinov Voenmekh Baltic State Technical University, St. Petersburg, 190005 Russia; dsci@mail.ru; vlademelyanov@gmail.com; mihailyakovchuk@gmail.com. Translated from Prikladnaya Mekhanika i Tekhnicheskaya Fizika, Vol. 56, No. 5, pp. 64–75, September–October, 2015. Original article submitted February 13, 2015; revision submitted May 13, 2015.

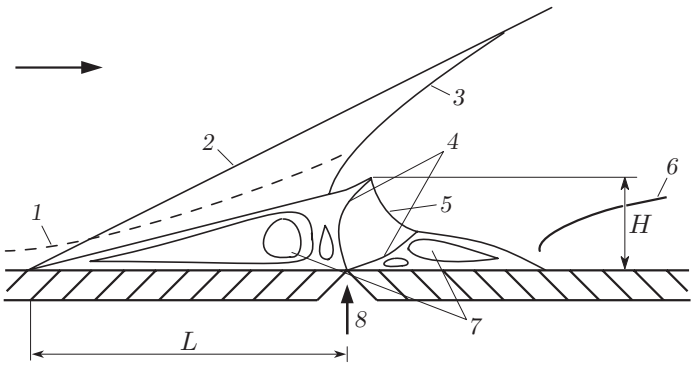

Fig. 1. Flow pattern resulting from transverse jet injection into a supersonic flow [10]: (*1*) turbulent boundary layer; (*2*) shock wave caused by separation; (*3*) bow shock wave; (*4*) barrel shocks; (*5*) Mach disk; (*6*) shock wave caused by repeated compression; (*7*) recirculation zone; (*8*) injection zone.

The intensity of the resulting shock waves and vortices is determined by the jet-to-crossflow pressure ratio, the crossflow Mach number, the form of the injection slot, the position of the injected jet, and a number of other parameters [3, 4, 13]. The mixing efficiency depends on the length of the separation zone L formed upstream of the injection slot and the depth of jet penetration into the crossflow H, which is determined by the position of the upper edge of the Mach disk.

Using engineering calculation methods, it is possible you to construct a simplified flow model and determine the main control parameters [10, 16, 17]. Many factors (unsteadiness, turbulence, thermal loads, separation of condensed-phase particles) that determine the degree of flow mixing are neglected in engineering calculations. To take them into account, it is needed to use computational fluid dynamics methods based on the Reynolds-averaged Navier–Stokes equations (RANS).

An overview of different approaches to the modeling of turbulence, such as large eddy simulation (LES), detached eddy simulation (DES), and combined approaches (LES/RANS), is given in [1]. The results of physical experiments conducted over wide ranges of Mach and Reynolds numbers ($M_\infty = 2$–13 and $Re = 7.5 \cdot 10^6$–$5.5 \cdot 10^8$) and ratios of the pressures in the injected gas jet and supersonic crossflow are presented in [18, 19].

The influence the choice of the turbulence model and the width of the jet injection slot on the calculated results is discussed in [20–22]. The calculation results obtained in [23] using the SST turbulence model are in good agreement with experimental data [14, 24]. Similar results obtained in [2] were compared with data [18, 19]. The model of transfer of Reynolds stresses provides more accurate results compared to the standard k–ε model of turbulence and its modifications [25]. The topology of the three-dimensional flow induced by normal injection of an underexpanded jet into subsonic and supersonic flows is studied in [12].

The approaches used in [1, 26–30] to model the interaction between an transverse jet with a supersonic flow allow a highly detailed study of the evolution of the shock-wave and vortex structures of the flow [1]. In the calculations, domains of great length and sufficiently detailed grid are used. In particular, Kawai and Lele [26, 27] performed LES calculations in a domain which has relative dimensions of $10.0 \times 3.3 \times 4.0$ (the diameter of the injection slot is used as the characteristic length) on a grid comprising $38 \cdot 10^6$ cells. Peterson and Candler [29] performed DES calculations using a grid containing $13.8 \cdot 10^6$ cells, with relative dimensions of the computational domain of $35 \times 16 \times 8$.

Interaction between an oblique shock wave resulting from supersonic flow over an inclined ramp in a channel and an injected jet has been investigated by Huang et al. [31]. The jet was injected through a slot in the bottom wall of the channel, and the ramp was located on the top wall upstream of the slot. In the numerical calculations, the position of the ramp in the channel and the size and angle of inclination of the ramp to the incoming were varied. The geometric model used was similar to that in [18], and the calculations were carried out for $p_j/p_\infty = 8.75$, 63, and 50 using different turbulence models at small (RNG k–ε model) and large (SST model) pressure differences in the jet and the crossflow [22]. Interaction between an oblique shock wave and a jet injected into a supersonic flow, the resulting three-dimensional flow structure, and the mixing and combustion mechanisms are considered in [32]

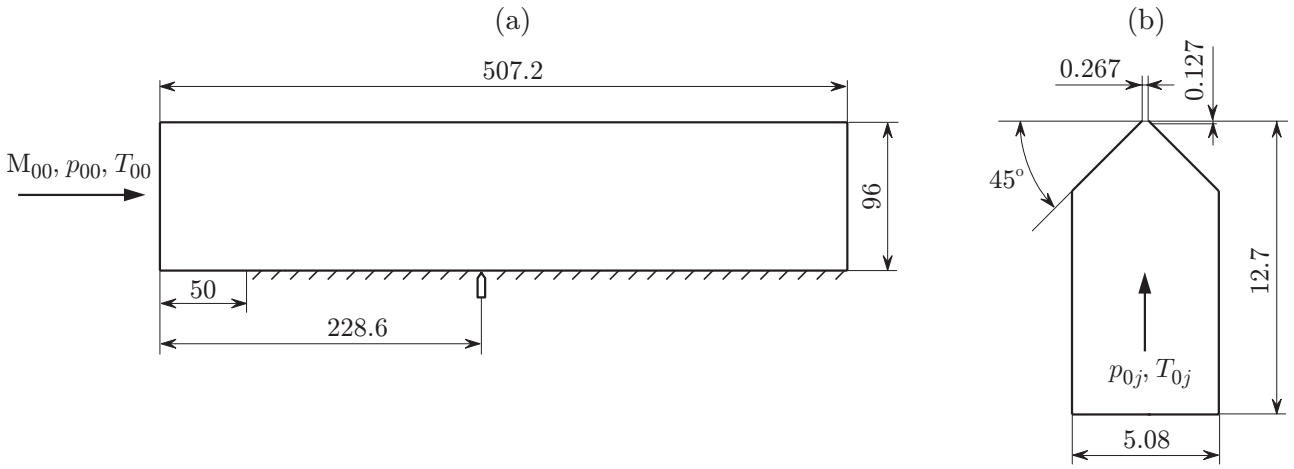

Fig. 2. Geometry of the computational domain (a) and slot nozzle (b).

on the basis of the results of physical and numerical experiments. Fedorova et al. [33] carried out calculations using the SST turbulence model for large values of the total temperature of the flow.

Parametric studies and the choice of optimal problem parameters are usually based on solving the RANS equations. Despite the large amount of available data on the interaction of a transverse jet with a supersonic flow, there is a need to analyze the applicability of different turbulence models. In this paper, using the results of numerical and physical experiments, we compare the accuracy of different turbulence models (the Spalart–Allmaras model, the implementable k–ε model, the k–ω model, and the SST model) and analyze the possibility of using these models. The injection slot nozzle is included in the computational domain to improve the calculation accuracy and formulate reasonable boundary conditions in the cross section through which the jet is injected.

1. GEOMETRY AND BOUNDARY CONDITIONS

Consider the interaction between a jet injected through a flat slot in a plate with velocity U_j and an undisturbed supersonic flow moving parallel to the plate and having velocity U_∞. The flow pattern is characterized by the ratio of dynamic pressures in the injected jet and the crossflow [10]. For an ideal gas, this ratio is written as

$$J = \frac{\rho_j U_j^2}{\rho_\infty U_\infty^2} = \frac{\gamma_j p_j \mathrm{M}_j^2}{\gamma_\infty p_\infty \mathrm{M}_\infty^2}.$$

The subscripts j and ∞ correspond to the injected jet and the crossflow in the channel.

The computational domain comprising the main channel and the slot nozzle is shown schematically in Fig. 2. The length of the plate is 507.2 mm, and the height of the computational domain is 96 mm. The distance from the front edge of the plate to the line of symmetry of the slot nozzle is equal to 228.6 mm. The jet is injected from the surface of the flat plate along the normal to the undisturbed flow through a flat slot nozzle 0.267 mm wide and 152.4 mm long. Side plates are mounted at the edges of the nozzle to provide plane flow. The origin of the Cartesian coordinate system is at the center of the injection slot. The coordinate x is measured in the direction of flow propagation.

At the boundary through which the main flow enters the computational domain, we specify the Mach number M_∞, the static pressure p_∞, the static temperature T_∞, and turbulence characteristics (the turbulence intensity is 1%, and the characteristic scale of turbulence is 0.1 mm). The boundary conditions on the boundary of the input slot nozzle are the total pressure p_{0j}, the total temperature T_{0j}, and turbulence characteristics (the turbulence intensity is 0.1%, and the hydraulic diameter is 0.532 mm). The no-slip and no-flow boundary conditions for the tangential and normal velocity components are imposed on the plate surface and the nozzle walls, and slip conditions (inviscid wall) are imposed on the upper boundary and the region of the computational domain upstream of the plate. The surface of the plate and the walls of the slot nozzle are considered thermally insulated.

Table 1. Flow and jet parameters in the inlet section of the computational domain

Experiment number	M_∞	$p_{0\infty}$, Pa	$T_{0\infty}$, K	p_{0j}, Pa	T_{0j}, K
2	2.61	133 758	317.8	159 269	297.8
3	2.61	132 035	317.8	299 922	294.4
4	2.61	133 069	317.8	572 955	291.1
5	2.61	133 758	318.3	1 044 556	288.3
13	3.50	240 627	314.4	379 901	291.7

Table 2. Characteristics of different computational grids

Grid	N_1	N_2	N_3	N
1	61	117	61	194 880
2	133	229	133	633 600
3	269	229	133	125 376
4	537	457	265	501 504

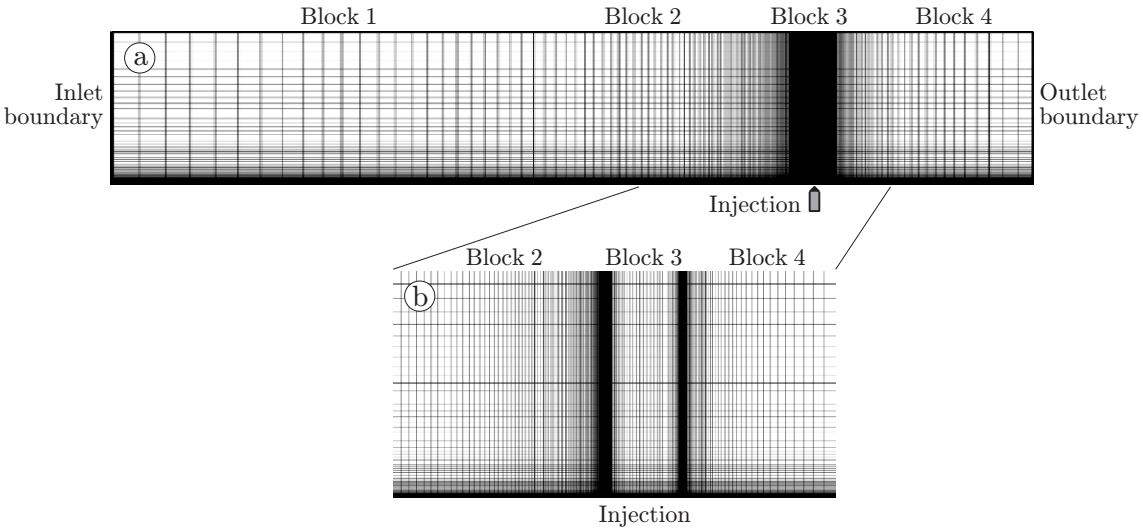

Fig. 3. Computational grid 1 (a) and its fragment (b).

The turbulence characteristics on the wall are determined using method of wall functions. In the outlet, the flow characteristics are found by extrapolating their values from the internal nodes of the grid (free outflow conditions).

The numerical experiment consists of a number of calculation corresponding to five injection modes. For ease of comparison of the results of the numerical simulation and experimental data, we use the designations of the calculation variants and control points adopted in [18]. The parameters of the physical and computational experiments are shown in Table 1 (Mach number, total pressure, and total temperature of the main flow and the injected gas).

The working media are air (main flow) and nitrogen (injected medium). Reference thermal characteristics of the media are used.

2. COMPUTATIONAL GRIDS

The calculations are carried out on four block-structured grids with different resolutions, whose characteristics are given in Table 2 (N_1 is the number of grid nodes in the inlet section of the computational domain, N_2 is the number of nodes on the plate upstream of the slot, N_3 is the number of nodes on the plate downstream of the slot, and N is the number of nodes).

Figure 3 shows grid 1 used in the calculation. The grid consists of four blocks that correspond to the undisturbed flow upstream of the plate (block 1), the flow upstream of the injection slot (block 2), the slot nozzle (block 3), and the flow downstream of the injection slot (block 4). In each block, the grid spacing on the x axis is non-uniform (the initial grid spacing varies from block to block). On the y axis, the grid is refined toward the surface of the plate (in all blocks, the grid nodes in the y direction are distributed equally). The slot nozzle contains 45 nodes along the width and 77 nodes along the height.

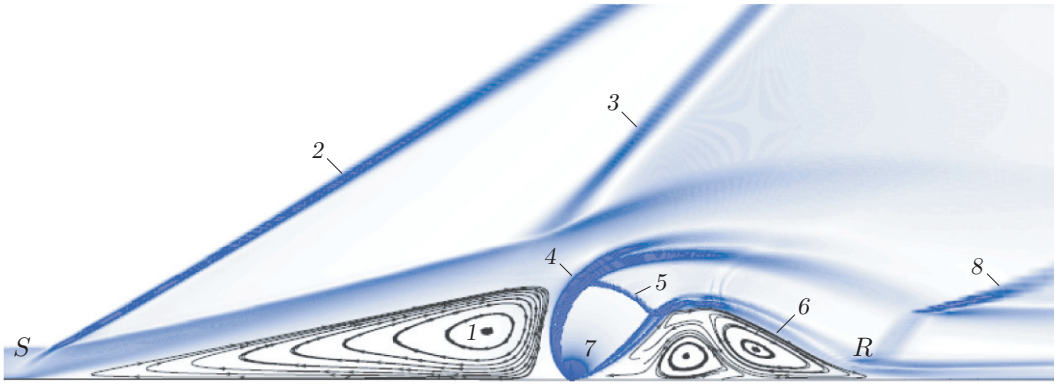

Fig. 4. Results of numerical simulation of the jet flow in the steady-state mode: (*1*) front stagnation zone; (*2*) bow shock wave; (*3*) shock wave over the injection slot; (*4, 8*) barrel shock waves; (*5*) Mach disk; (*6*) stagnation zone of reduced pressure; (*7*) region of jet penetration into the supersonic flow.

Grids 1–3 have the same near-wall spacing equal to 10^{-6} m. Grid 4 is generated by adding nodes to grid 3 and reducing the size of all of its cells. On grid 4, the first layer of nodes is located at a distance of $5 \cdot 10^{-7}$ m from the surface of the plate. For grids 1–3, the near-wall coordinate y^+ varies in the range of 0.008–2.660, and for the grid 4, in the range of 0.003–1.700; the coordinate y^+ takes maximum values near the front edge of the plate. Increasing the pressure difference in both the injected jet and the crossflow leads to some increase in the maximum value of the coordinate y^+. In particular, in passing from grid 2 to grid 4, the maximum value of the wall coordinate increases by about 25%.

In the calculations, laminar–turbulent transition is not modeled. Data of physical experiment [18] show that for all modes of jet injection into the flow, the transition area is located upstream of the slot nozzle. Laminar–turbulent transition in the boundary layer occurs at a distance from the front edge of the plate equal to 50.8–76.2 mm.

3. COMPUTATIONAL PROCEDURE

In the calculations, we use the Ansys Fluent package based on Reynolds averaged Navier–Stokes equations. The equations are closed using different differential turbulence models (the Spalart–Allmaras model, the implementable k–ε model, the k–ω model, and the SST model). The convection and diffusion equations are solved for each of the gases to take into account the mixing of flows of dissimilar gases.

Discretization of the basic equations is carried out using the finite volume method and the SIMPLE pressure correction method. Discretization of convective and diffusive fluxes is accomplished using second-order counterflow and centered finite difference schemes with the Roe flux vector splitting, and time discretization is performed using an implicit scheme of second-order accuracy. The system of difference equations is solved by the lower-upper symmetric Gauss–Seidel (LUSGS) method [34]. The Courant number is Ku = 2–7.

The convergence of the iterative process is controlled by checking the level of discrepancy of the desired functions and the satisfaction of the integral continuity equation. The calculations are stopped at the moment when the level of discrepancy of the desired functions is reduced by three orders of magnitude, and the difference of the mass fluxes at the inlet and outlet boundaries of the computational domain becomes less than 10^{-3} kg/s.

4. FLOW STRUCTURE

The results of the numerical simulation corresponding to the steady-state flow are shown in Fig. 4 (experiment 4). Qualitatively, the flow pattern is similar to the pattern obtained in calculations based on other turbulence models [22], which is shown in Fig. 1.

The flow slows down upstream of the injected jet, which serves as an obstacle to the crossflow, resulting in a positive pressure gradient (a high-pressure region is formed upstream of the injection slot, and a low-pressure region

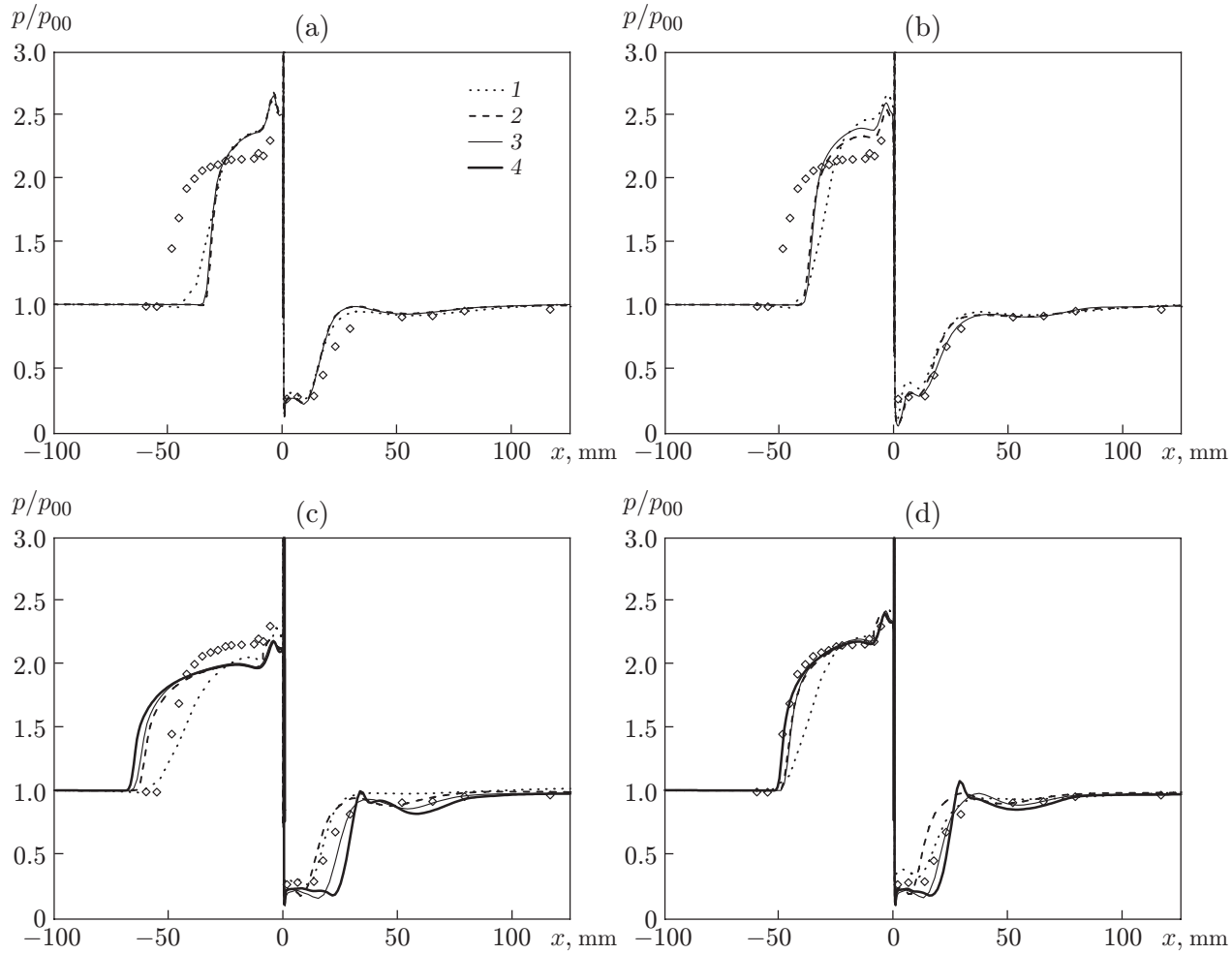

Fig. 5. Wall pressure distribution obtained using different turbulence models on different grids: (a) Spalart–Allmaras model; (b) implementable k–ε model; (c) k–ω model; (d) SST model; (*1*) calculation on grid 1; (*2*) calculation on grid 2; (*3*) calculation on grid 3; (*4*) calculation on grid 4; the points are experimental data [18].

is formed downstream of it) which causes separation of the boundary layer at the point S. This produces a front stagnation zone *1* and a bow shock wave *2*. The crossflow streamlines rotate when passing through the bow shock wave and the shock *3* over the injection slot. The injected jet is bent under the influence of the crossflow (near the surface of the plate, the jet streamlines rotate through a larger angle) and come in contact with the streamlined surface at the point R at some distance downstream of the slot, resulting in the formation of a stagnation zone *6* of reduced pressure. Repeated compression of the flow give rise to a shock wave *8* downstream of the point R. Region *7* (the region of jet penetration into the supersonic flow) is bounded by two barrel shock waves *4* and a Mach disk *5*.

The thickness of the boundary layer is substantially greater than the width of the slot, so that expansion of the jet occurs in the region of flow separation. In this case, the interaction of the flow with the wall is determined by the viscosity. Jet injection leads to separation of the turbulent boundary layer and a redistribution of the pressure on the plate. The separation zones can be calculated using a semi-empirical model [16, 17].

5. COMPARISON OF TURBULENCE MODELS

Figure 5 shows static pressure distributions along the plate surface calculated on different grids with different resolution using different turbulence models and the results of a physical experiment [18]. The calculations were

performed for the inlet flow parameters corresponding to experiment 4 (see Table 1). Calculations on grid 4 using the Spalart–Allmaras models and the implementable k–ε models were not carried out.

The calculation results obtained using different turbulence models have a feature in common: for grids 2–4, the pressure distribution on the plate surface is almost independent of the resolution of the grid. In all calculations on a coarse grid (grid 1), the same position of the separation point was obtained, and maximum pressure values correspond to the values calculated on more detailed grids (grids 2–4). The fullness of the wall pressure profiles corresponding to grid 1 and grids 2–4 is different. On grid 1, the pressure profile is less filled than that on grids 2–4. Similar results were obtained in [22].

The most significant differences between the results obtained in coarse and detailed grids are observed when using the standard k–ω model (see Fig. 5c). In this case, the pressure profile obtained on grid 1 is less filled than the pressure profile obtained on grids 2–4 and the pressure values are too low compared to the corresponding values calculated for other turbulence models. The plateau region obtained in the experiment and reproduced when using detailed grids is absent in the calculations on grid 1.

The Spalart–Allmaras model (see Fig. 5a) incorrectly determines the position of the separation point of the boundary layer. Furthermore, the separation of the boundary layer occurs later than in the calculations for the other turbulence models (the separation point moves downstream), the pressure profile is less filled, and a plateau region is absent.

Calculations based on the implementable k–ε model (see Fig. 5b) give results similar to the results obtained using the Spalart–Allmaras model (except the plateau region).

The best agreement between the calculated results and the data of the physical experiment is obtained when using the SST turbulence model (see Fig. 5d). The pressure distribution calculated on the coarse grid (grid 1) is consistent with sufficient accuracy with experimental data [18]. Further calculations were performed using the SST turbulence model.

Important characteristics of the fuel and oxidizer mixing and combustion of the mixture in a supersonic flow is the length of the recirculation zone and the depth of jet penetration [30]. The length of the recirculation zone formed upstream of the injection slot and the jet penetration depth in a supersonic flow calculated using different models turbulence are shown in Fig. 6. Increasing the pressure gradient increases the length the recirculation zone and the jet penetration depth in the flow. The influence of the turbulence models on the jet penetration depth is less significant than their influence on the size of the recirculation zone.

The SST model provides not only pressure distributions consistent with the data of the physical experiment, but also fairly accurate values of the length of the recirculation zone located upstream of the injection slot. The Spalart–Allmaras model and the implementable k–ε model give overestimate the length of the recirculation zone, and the standard k–ω model underestimates the length of the recirculation zone (the resolution of the computational grid has little effect). Similar results were obtained in [22].

The wall pressure distributions and the length of the recirculation zone obtained using the SST model are weakly dependent on the resolution of the grid. The wall pressure distribution corresponding to the recirculation zone downstream of the injection slot depends more significantly on the grid resolution. The solution obtained using the SST model and grid 4 is in good agreement with experimental data [18].

6. COMPARISON OF CALCULATION VARIANTS

The SST turbulence model was used in calculations with different types of boundary conditions (see Table 1). Figure 7 shows the static pressure distributions on the plate surface under different conditions of jet injection into a supersonic flow (curves). As the intensity of injection is increased, the separation point of the boundary layer is shifted upstream (to the left from the slot injection). In this case, the pressure profile becomes more filled, and the plateau region more pronounced. Maximum values of the wall pressure change slightly.

The results of the numerical simulation agree well with the experimental data for all injection modes, confirming the usefulness of the SST turbulence model for solving similar problems in a wide range of parameters of the cross flow and the injected jet. Some difference in the results corresponding to mode 5 are due to the fact that in the experiment with this injection mode, boundary layer separation occurs upstream of the edges of the side

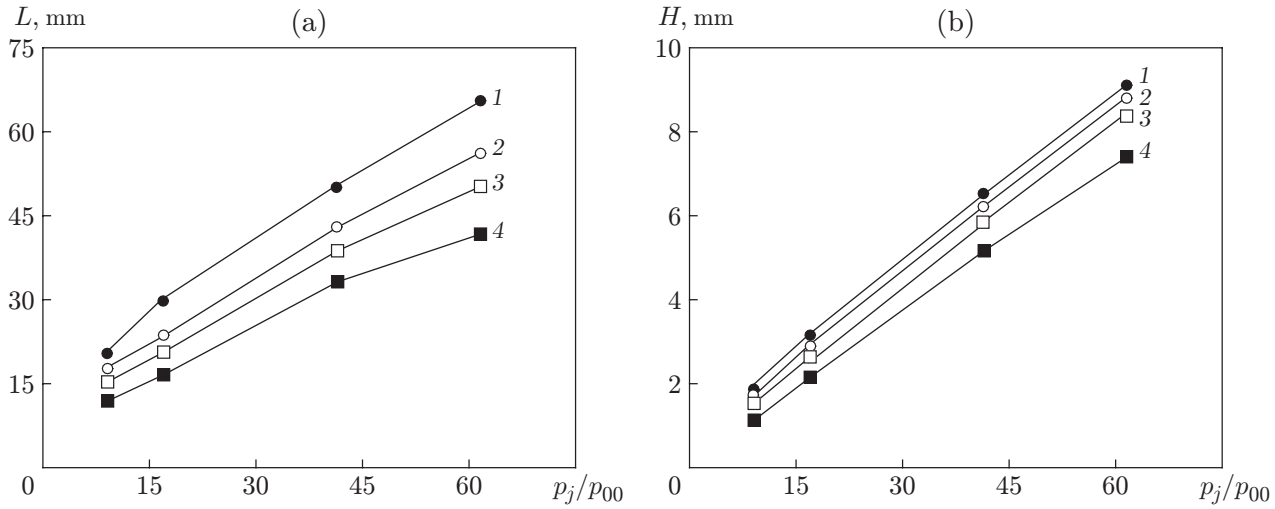

Fig. 6. Length of the front recirculation zone (a) and the jet penetration depth in the flow (b) calculated for different turbulence models: (*1*) SST model; (*2*) implementable k–ε model; (*3*) Spalart–Allmaras model; (*4*) k–ω model.

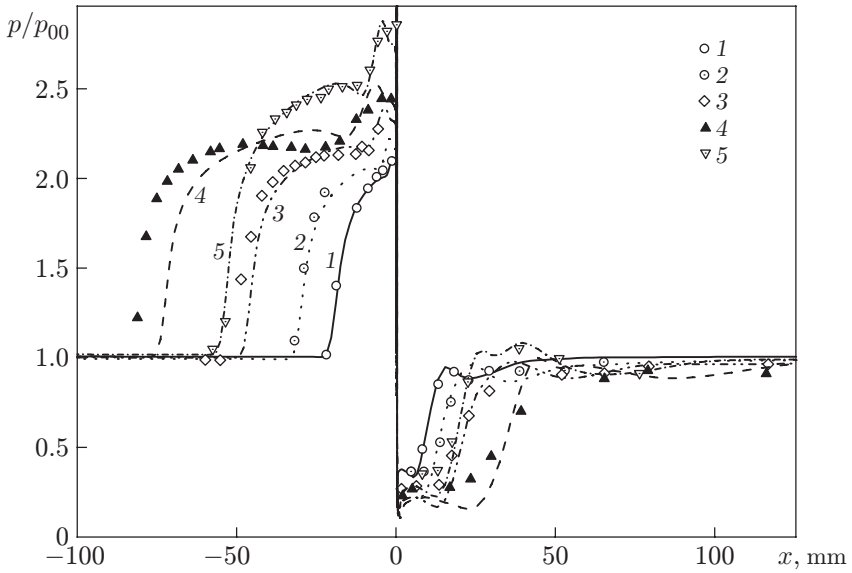

Fig. 7. Results of numerical simulations (curves) and physical experiment [18] (points) for jet injection into a supersonic flow: (*1*) mode 2; (*2*) mode 3; (*3*) mode 4; (*4*) mode 5; (*5*) mode 13.

plates mounted on the sides of the slot nozzle. The separated boundary layer interacts with the plates to give rise to shock waves, and the flow becomes substantially three-dimensional. To account for these features, it is necessary to solve the three-dimensional problem.

CONCLUSIONS

Numerical simulation of the flow resulting from jet injection through a slot nozzle into a supersonic flow was performed. In the calculations, the static pressure difference in the injected jet and the crossflow was varied. The

calculations were performed on a grid with different resolutions using the Spalart–Allmaras turbulence model, the implementable k–ε model, the k–ω model, and the SST model.

The applicability of different turbulence models and the accuracy of calculations based on them were analyzed by comparing the calculated and experimental data on the wall pressure distribution, the length of the recirculation zone, and the depth of jet penetration in supersonic flow. The SST model yields results in good agreement with the data of the physical experiment in a wide range of parameters characterizing the jet injection.

REFERENCES

1. E. Hassan, J. Boles, A. Hikaru, et al., "Supersonic Jet and Crossflow Interaction: Computational Modeling," Progr. Aerospace Sci. **57** (1), 1–24 (2013).
2. M. S. Yakovchuk, "Numerical Simulation of the Dynamic Processes of Jet Injection into the Supersonic Part of a Nozzle," Vestn. Samar. Gos. Aerokosm. Univ., No. 3, 359–367 (2012).
3. A. R. Karagozian, "Transverse Jets and Their Control," Progr. Energy Combust. Sci. **36** (5), 531–553 (2010).
4. K. Mahesh, "The Interaction of Jets with Crossflow," Annual Rev. Fluid Mech. **45**, 379–407 (2013).
5. R. I. Sykes, W. S. Lewellen, and S. F. Parker, "On the Vorticity Dynamics of a Turbulent Jet in a Crossflow," J. Fluid Mech. **168**, 393–413 (1986).
6. T. F. Fric and A. Roshko, "Vortical Structure in the Wake of a Transverse Jet," J. Fluid Mech. **279**, 1–47 (1994).
7. H. Johari, M. Pacheco-Tougas, and J. C. Hermanson, "Penetration and Mixing of Fully Modulated Turbulent Jets in Crossflow," AIAA J. **37** (7), 842–850 (1999).
8. T. T. Lim, T. H. New, and S. C. Luo, "On the Development of Large-Scale Structures of a Jet Normal to a Crossflow," Phys. Fluids **13** (3), 770–776 (2001).
9. C. J. Roy and F. G. Blottner, "Review and Assessment of Turbulence Models for Hypersonic Flows," Progr. Aerospace Sci. **42** (7/8), 469–530 (2006).
10. J. A. Schetz and F. S. Billig, "Penetration of Gaseous Jets Injected into a Supersonic Stream," J. Spacecraft Rockets **3** (11), 1658–1665 (1966).
11. A. Ben-Yakar, M. G. Mungal, and R. K. Hanson, "Time Evolution and Mixing Characteristics of Hydrogen and Ethylene Transverse Jets in Supersonic Crossflows," Phys. Fluids **18** (2), 026101 (2006).
12. D. A. Dickmann and F. K. Lu, "Shock/Boundary Layer Interaction Effects on Transverse Jets in Crossflow over a Flat Plate," AIAA Paper No. 2008-3723 (Seattle, 2008).
13. M. R. Gruber, A. S. Nejad, T. H. Chen, and J. C. Dutton, "Large Structure Convection Velocity Measurements in Compressible Transverse Injection Flow-Fields," Exp. Fluids **22** (5), 397–407 (1997).
14. B. Stahl, H. Emunds, and A. Gülhan, "Experimental Investigation of Hot and Cold Side Jet Interaction with a Supersonic Cross-Flow," Aerospace Sci. Technol. **13** (8), 488–496 (2009).
15. N. Qin and A. Redlich, "Massively Separated Flows due to Transverse Sonic Jet in Laminar Hypersonic Stream," Shock Waves **9** (2), 87–93 (1999).
16. A. M. Teverovskii, "Approximate Calculation of the Flat Interaction of a Side Jet with a Supersonic Flow," Tr. Tsentr. Inst. Aviats. Motorostr., No. 482, 4–12 (1971).
17. G. F. Glotov and O. M. Kolesnikov, "Approximate Calculation of the Two-Dimensional Interaction of a Transverse Jet with a Supersonic Flow in Combustion at the Front Separation Point," Tr. Tsentr. Aerogidrodinam. Inst., No. 1736, 3–14 (1976).
18. F. W. Spaid and E. E. Zukoski, "A Study of the Interaction of Gaseous Jets from Transverse Slots with Supersonic External Flows," AIAA J. **6** (2), 205–212 (1968).
19. F. W. Spaid, "Two-Dimensional Jet Interaction Studies at Large Values of Reynolds and Mach Numbers," AIAA J. **13** (11), 1430–1434 (1975).
20. R. Dhinagaran and T. K. Bose, "Numerical Simulation of Two-Dimensional Transverse Gas Injection into Supersonic External Flows," AIAA J. **36** (3), 486–488 (1998).
21. A. T. Sriram and J. Mathew, "Improved Prediction of Plane Transverse Jets in Supersonic Crossflows," AIAA J. **44** (2), 405–407 (2006).
22. W. Huang, W. D. Liu, S. B. Li, et al., "Influences of the Turbulence Model and the Slot Width on the Transverse Slot Injection Flow Field in a Supersonic Flows," Acta Astronaut. **73**, 1–9 (2012).

23. G. Aswin, D. Chakraborty, "Numerical Simulation of Transverse Side Jet Interaction with Supersonic Free Stream," Aerospace Sci. Technol. **14** (5), 295–301 (2010).
24. B. Stahl, H. Esch, and A. Gülhan, "Experimental Investigation of Side Jet Interaction with a Supersonic Cross Flow," Aerospace Sci. Technol. **12** (4), 269–275 (2008).
25. C. F. Chenault, P. S. Beran, and R. D. W. Bowersox, "Numerical Investigation of Supersonic Injection Using a Reynolds-Stress Turbulence Model," AIAA J. **37** (10), 1257–1269 (1999).
26. S. Kawai and S. K. Lele, "Mechanisms of Jet Mixing in a Supersonic Crossflow: A Study Using Large-Eddy Simulation," AIAA Paper No. 2008-4575 (Reston, 2008).
27. S. Kawai and S. K. Lele, "Large-Eddy Simulation of Jet Mixing in Supersonic Crossflows," AIAA J. **48** (9), 2063–2083 (2010).
28. S. H. Won, I. S. Jeung, B. Parent, and J. Y. Choi, "Numerical Investigation of Transverse Hydrogen Jet into Supersonic Crossflow Using Detached-Eddy Simulation," AIAA J. **48** (6), 1047–1058 (2010).
29. D. Peterson and G. Candler, "Simulations of Mixing for Normal and Low-Angled Injection into a Supersonic Crossflow," AIAA J. **49** (12), 2792–2804 (2011).
30. Z. A. Rana, B. Thornber, and D. Drikakis, "Transverse Jet Injection into a Supersonic Turbulent Cross-Flow," Phys. Fluids **23** (4), 046103 (2011).
31. W. Huang, Z.-G. Wang, J.-P. Wu, and S.-B. Li, "Numerical Prediction on the Interaction between the Incident Shock Wave and the Transverse Slot Injection into a Supersonic Flows," Aerospace Sci. Technol. **28** (1), 91–99 (2013).
32. T. Mai, Y. Sakimitsu, H. Nakamura, et al., "Effect of the Incident Shock Wave Interacting with Transversal Jet Flow on the Mixing and Combustion," Proc. Combust. Inst. **33** (2), 2335–2342 (2011).
33. N. N. Fedorova, I. A. Fedorchenko, and A. V. Fedorov, "Mathematical Modeling of Jet Interaction with a High-Enthalpy Flow in an Expanding Channel," Prikl. Mekh. Tekh. Fiz. **54** (2), 32–45 (2013) [J. Appl. Mech. Tech. Phys. **54** (2), 195–206 (2013).
34. A. Jameson, S. Yoon, "Lower-Upper Implicit Schemes with Multiple Grids for the Euler Equations," AIAA J. **25**, 929–935 (1987).